Flexible and High Temperature Supercapacitor Based on Laser-Induced Graphene Electrodes and Ionic Liquid Electrolyte, a De-rated Voltage Analysis.

(Article begins on next page)

23 April 2024

Flexible and High Temperature Supercapacitor Based on Laser-Induced Graphene Electrodes and Ionic Liquid Electrolyte, a De-rated Voltage Analysis.

Pietro Zaccagnini[a,b], Daniele di Giovanni[a], Manuel Gomez Gomez[a], Stefano Passerini[c,d], Alberto Varzi[c,d]*, Andrea Lamberti[a,b]*

[a]*Politecnico di Torino, Dipartimento di Scienza Applicata e Tecnologia (DISAT), Corso Duca Degli Abruzzi, 24, 10129 Torino, Italy*
E-mail: andrea.lamberti@polito.it
[b]*Istituto Italiano di Tecnologia, Center for Sustainable Future Technologies, Corso Trento, 21, 10129 Torino, Italy*
[c]*Helmholtz Institute Ulm (HIU) Helmholtzstrasse 11, 89081 Ulm, Germany*
[d]*Karlsruhe Institute of Technology (KIT), P.O. Box 3640, 76021 Karlsruhe, Germany*
E-mail: alberto.varzi@kit.edu

Keywords: laser-induced graphene, ionic liquid, micro-supercapacitor, flexible, high temperature

Abstract

Herein we report the fabrication and electrochemical characterization of a novel type of supercapacitor composed of laser-induced graphene (LIG) electrodes, achieved by the laser-writing of polyimide foils, and 1-Butyl-1-methylpyrrolidinium bis(trifluoromethanesulfonyl)imide ionic liquid as electrolyte. This combination allows the development of a flexible microsupercapacitor suitable for harsh environment application. The influence of several parameters is evaluated with the aim of maximizing the performance of the flexible pouch-bag devices, such as the laser-writing conditions, type of electrode layout and amount of nitrogen-doping. Among them, the laser writing conditions are found to strongly influence the areal capacitance allowing to achieve about 4 mF cm^{-2}, as measured from the galvanostatic charge-discharge measurement at 10 µA cm^{-2}, with a maximum operating potential range of 3 V at 25 °C.

In order to probe the potential application of such device, i) flexible pouch architecture and ii) high temperature measurements (considering harsh environment field) are investigated. This type of flexible device exhibits energy and power density as high as 4.5 µWh cm-2 and 90.5

µW cm-2, respectively, high cycling stability as well as acceptable coulombic efficiency above 97% demonstrating good stability even at high bending condition (1.25 cm of bending radius). The electrochemical measurements increasing temperature up to 100 °C reveal a 300% of rise in capacitance and 43% of increment in energy density at de-rated voltage. The obtained energy storage performance are comparable to the best data ever reported for a microsupercapacitor for high temperature application. Moreover, a de-rated voltage analysis (DVA) is proposed as a safe procedure to characterize an energy storage device in an extended temperature range without compromising the system performances.

1. Introduction

Supercapacitors (SCs), and in particular their miniaturized family known as microsupercapacitors (MSCs), are considered to be the most promising candidates toward light-weight, portable and reliable energy storage devices able to work at low-/ultra-low power scale, thanks to their intrinsic advantages such as wide power density range, fast charging-discharging rate and long cycling life.[1,2] However, increasing the operating temperatures is essential for harsh environment applications such as automotive, aerospace, solar/wind energy integration, or in general to enhance the safety of the devices in view of wearable or implantable applications. Indeed, consumer electronics requires the power source to be compliant to the temperature range -20°C +85°C, while an extension up to +125°C for automotive applications and down to -55°C for military field must be considered. [3,4]

MSCs can be designed in order to be fully compliant to these ranges, simply by using the appropriate electrolyte, as reported in the work of Lin and co. workers.[5] Among the electrolytes available for supercapacitors, ionic liquids (room temperature molten salts) are very appealing due to their negligible vapour pressure and high thermal degradation threshold if compared to solutions of conventional organic solvents commonly used for supercapacitors (such as, e.g., propylene carbonate or acetonitrile).[6,7]

2

In this work we propose the fabrication of a flexible MSC including electrodes of laser-induced graphene (LIG) obtained on polyimide (PI) substrate, and featuring the ionic liquid (IL) 1-Butyl-1-methylpyrrolidinium bis(trifluoromethanesulfonyl)imide [PYR14][TFSI] as the electrolyte. Concerning the state of the art of ILs, [PYR14][TFSI] was selected instead of BF4 or PF6 anion based ILs because of the higher chemical stability of the TFSI anion. Moreover, the higher electrochemical and thermal stability makes [PYR14][TFSI] a suitable choice for the purpose of this study.

LIG intrinsically answer to all the previously cited issues being written on flexible polyimide foil, thermally stable up to 300°C, while the IL represents the best compromise among electrochemical properties, thermal stability, safety, and recyclability.

PI is a very well-known polymer in the electronics field because it is used as chemical, thermal and electrical insulating layer for electronic boards and it is subject to laser manufacturing in order to be patterned according to electronic boards profiles and features. By exposing PI to high power concentrated laser pulses, it can be converted in a graphitic material known as laser-induced graphene, firstly demonstrated by Tour et al. in 2014.[8] By playing with laser parameters it is possible to tune material properties as proved by Lamberti et al.[9] As demonstrated in the latter work, by tuning laser power, frequency and scan speed it is possible to obtain several morphological structures and different carbon doping levels due to nitrogen residuals. Here we propose a study of three different morphologies in IL environment at room temperature and the characterization of the best performing device at temperatures as high as 100°C, being limited only by the pouch cell packaging.

It is very well known that electrical properties of SCs varies with temperature[10] and, in particular, with increasing temperature the capacitance increase, while Equivalent Series Resistance (ESR) and the electrochemical stability window of the electrolyte decrease. Although the first two temperature effects are positive, the reduction of operative voltage poses a limit to the energy and power capability. In practical operations, devices cannot be let

operate in a temperature dependent voltage window for the main reason that self-discharge (due to leakage currents) increases with voltage and temperature. In the case of electric double-layer capacitors (EDLCs),[11] this is mainly because these devices store electrostatic potential energy with no thermodynamic and kinetic mechanisms stabilizing the potential difference, as it occurs in batteries. Thus, keeping the State of Charge (SoC) of a SC might lead to complex electronics especially if the electrical properties dynamically change with temperature.[11] With this work we want also to propose, for the first time to the best of our knowledge, a temperature characterization based on de-rated voltage analysis (DVA). In this way it is possible to investigate the device properties by keeping fixed one of two thermodynamic quantities, i.e. the voltage, in order to better appreciate temperature effects. Our DVA analysis is aimed to avoid the behaviour that Hibino and co-workers found at 200°C working at relatively high rates. They observed an energy density drop at 4.5-6 A g^{-1}, 1 V voltage window, implying a decrease in the discharge capacitance.[12] Indeed, from the reported impedance spectroscopy analysis it is clear that the device was irreversibly damaged.

2. Experimental

2.1 Materials synthesis

Laser Induced Graphene (LIG) electrodes were fabricated with an EOX 30W laser system provided by Datalogic. According to specifications, this laser system relies on the Pulsed Width Modulation (PWM) control of the laser source whose period is set through the frequency parameter and Duty Cycle (DC) by power parameter expressed as a percentage value. The laser output is calibrated to deliver a P_{rms} = 30 W at 5 kHz with duty cycle = 100 %. The output of the laser follows the PWM signal with a rise time of 100 μs.

In order to obtain the different morphologies, the power was fixed to 6%. Needle- and sheet-type morphologies were obtained by maintaining the frequency at 4kHz and setting the

writing speed at 125 mm s^{-1} and 200 mm s^{-1}, respectively. The porous morphology was obtained with 20kHz frequency and 150 mm s^{-1} scan velocity.

In Figure S1 we report the Computer-Aided Design (CAD) of the laser scribed geometry, according to the aforementioned parameters.

2.2 Device assembly

LIG devices on PI substrate were first dried at 120°C. They were laid then on a laboratory glass slide substrate. Contacts with LIG pads to be brought outside the pouch cell were made by means of pressed Al foils fixed by Kapton tape. A Whatman Glass Fibre (GF) membrane Grade F, dried at 180°C, was soaked with [PYR14][TFSI] electrolyte and placed over the interdigitated electrodes. A silver-coated aluminum stripe was used in each cell as pseudo reference electrode to monitor the potential evolution of individual electrodes. The thickness of the Ag layer was around 100 nm and it was deposited by a sputtering process. Another laboratory glass slide was placed over the rinsed GF membrane. With this stack, the membrane is fully adhered on the electrodes upon pouch cell sealing procedure. Photographs of the device assembly can be found in the supporting information, in Figure S1.

2.3 Characterization

Concerning the physical characterizations of the produced materials, we refer to our previous work.[9] However, concerning morphological characterizations we report SEM images in the supporting information Figure S3.

Electrochemical characterizations were carried out with a VMP3 (Bio-Logic, France) multi-channel potentiostat/galvanostat at room temperature (20°C +/- 0.1 °C) and Metrohm Autolab (Metrohm, Netherlands) for high temperature characterizations together with an Arbin cycler BT2000 (Arbin Instruments, Texas – USA) for long term galvanostatic tests. Temperature measurements were run in a Memmert UN30 oven with side opening for cables, able to keep

constant temperature 5°C above room temperature and a control of 0.1°C, operating in natural convection. Cyclic Voltammetry (CV), Galvanostatic Charge and Discharge (GCD) and Electrochemical Impedance Spectroscopy (EIS) measurements were performed at open circuit voltage in order to characterize the devices. CV tests were mainly used to study the electrochemical stability of the electrolyte at low scan speed, 10 mVs^{-1}, for 50 cycles. GCD measurements were used to characterize device rate capabilities and derive the Ragone plot. Finally, EIS was employed to monitor temperature effects at the interfaces. EIS spectra were collected in the frequency range 1 MHz-10 mHz, five points per decades, with peak amplitude of 5 mV. Each device of different morphology was subjected to 50 CV cycles at 10 mV s^{-1} at three different maximum cell voltages (2 V, 2.5 V and 3 V) in order to evaluate the electrolyte stability window at room temperature. The latter analysis was also extended to GCDs carried out at 10μA cm^{-2}, 50 cycles per operative voltage.

Leakage current (LC) was evaluated by holding devices at rated potential for 24h at constant temperature.

Capacitances were derived from the energy, which was computed as

$$E = \int V(t)I(t)dt \tag{1}$$

and using

$$E = \frac{1}{2}\frac{Q^2}{C} \tag{2}$$

where

$$Q = \int I(t)dt \tag{3}$$

The power was calculated by applying

$$P = \frac{E}{\Delta t} \tag{4}$$

where Δt is the discharge time, since all the quantities were evaluated in the discharge period.

The same relations were employed in order to compute charging quantities.

Concerning temperature measurements, we decided to perform a voltage window characterization and not to keep the voltage fixed at room temperature in order to avoid problems due to accelerated ageing. Moreover, after studying the operative voltage window we characterized devices at constant voltage throughout the whole temperature range in order to de-couple potential induced accelerated aging to temperature one. These kinds of problems were observed in literature.[5,13]

2.4 De-rated voltage analysis

The voltage stability window of these devices is mainly determined, rated, at room temperature and it is dependent on the anodic and cathodic limits imposed by the electrodes electrolyte interfaces.

If one assumes the two electrodes interfaces to be described by the Butler-Volmer equation,[14] the application of a potential difference to the device will turn in a shift of the electrodes potentials at the interfaces towards the anodic and cathodic limits, with respect to their equilibrium value. In the former equation, these over-potentials are compared to thermal voltage, in the quotient $F\eta/(RT)$. The thermal voltage, $v_{th}=k_bT/q$, enters the ratio since the Faraday constant is $F=N_A\,q$ and that the gas constant is $R=N_A\,k_b$, being N_A the Avogadro's number, k_b the Boltzmann's constant and q the electrons' unit charge. Finally, we recall that equilibrium redox potentials vary with temperature according to the same quantity, as predicted by the Nernst equation.[14]

Concerning the experimental procedure, we kept constant the temperature step leading to a constant thermal voltage difference of $\Delta v_{th} = 1.7$ mV. Consequently, we chose to decrease the applied potential by 100 mV at each temperature, which is more than 50 times higher than Δv_{th} itself. The reason for this choice was driven by accounting that temperature increases processes kinetics. Each device was let reach thermal equilibrium in a period of at least 1 h prior to the electrochemical testing.

7

Then, for a proper device characterization throughout a temperature range, the voltage is kept constant at a voltage stability window rated at the upper temperature limit. This is done in order to evaluate the influence of the change of a thermodynamic variable only, the temperature. This approach was meant to reduce the effects coming from thermally induced degradation effects close to the voltage limit in isopotential conditions at a voltage rated at room temperature. This gives the possibility to study and design devices stable in a wide temperature range at reduced, de-rated, voltage so to preserve lifetime.

3. Results and discussion

Previous studies have demonstrated that by acting on the laser parameters it is possible to tune the morphology and the elemental composition of the LIG with obvious impact on its electrochemical performance in an aqueous electrolyte.[8,9] Now, we investigate the combination with an ionic liquid electrolyte in order to verify its exploitation for high voltage temperature applications. The three morphologies of LIG here investigated have been previously analyzed in detail in a aforementioned publication allowing to determine their physical-chemical properties.[9] Anyway, we recall the morphologies in the pictures reported in Figure S3. As reported in **Figure 1**a, a linear increase in the areal capacitance is observed when increasing the maximum cell voltage of the device. This might be ascribed to faradic contributions from residual pyrrolic N sites.[9,15] It is also possible to appreciate that the needle-like LIG provides the largest areal capacitance among the different morphologies. Coulombic efficiencies versus the applied voltage are reported in Figure 1b. In Figure 1c the CV profiles collected at 10 mV s^{-1} and at maximum investigated cell voltage (3 V) are shown. All three morphologies show a slightly resistive behavior, as testified by the partial distortion of the box-shaped voltammogram typical of an ideal EDLC. Small bumps can also be observed for the needle morphology, which may be associated to the interaction between the ionic molecules and the carbon surface as well as pore insertion at high voltages, as discussed in

literature.[16,17] Together with CVs, GCD under low current density was also employed to study the device performance as function of the maximum cell voltage. These tests were carried out at 10 µA cm^{-2} and their results are reported in Figure S4.
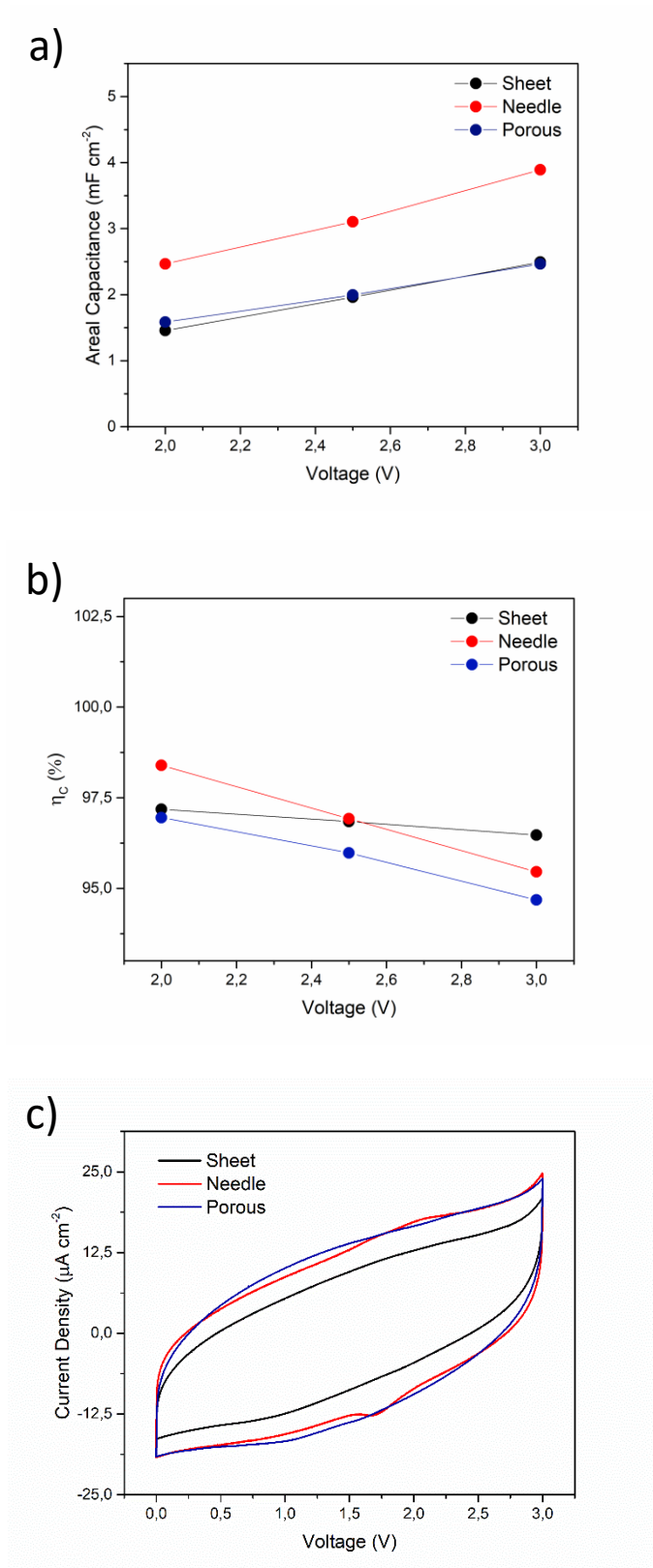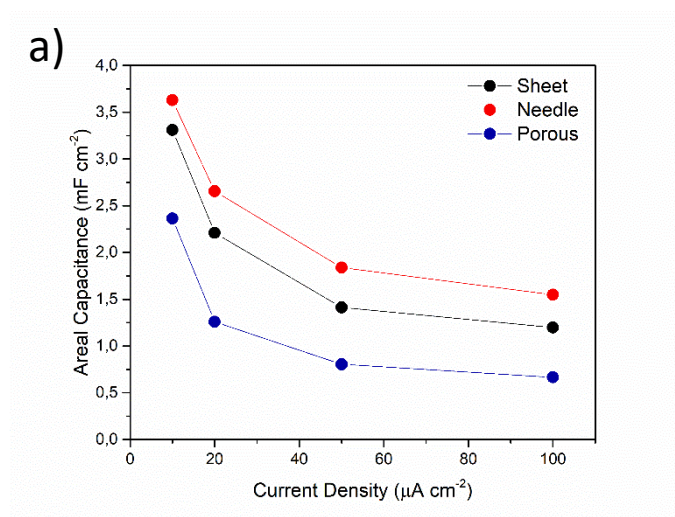
Figure 1. Comparison of areal capacitance (a) and coulombic efficiency (b) at increasing applied voltage during CV at 10 mV s^{-1}. (c) Overlay of CVs of different morphologies carried out at 10 mV s^{-1} with 3 V potential window.

From the potential evolution of the individual electrodes, it is clear that the different morphologies also show different capacitive behavior. Indeed, in the case of porous morphology the LIG electrodes appear strongly asymmetric, with substantially lower capacitance delivered by the positive electrode. We assumed this behavior to be due to apparent selective capacitive properties.

Afterwards, the GCD tests were performed at increasing current density (10, 20, 50 and 100 $\mu A\ cm^{-2}$, 100 cycle each) in order to evaluate the rate capability of the fabricated devices. These current density values were chosen according to the average values observed in the voltammograms. Moreover, these current rates have been demonstrated to be required in the energy harvesting scenario.[18,19]
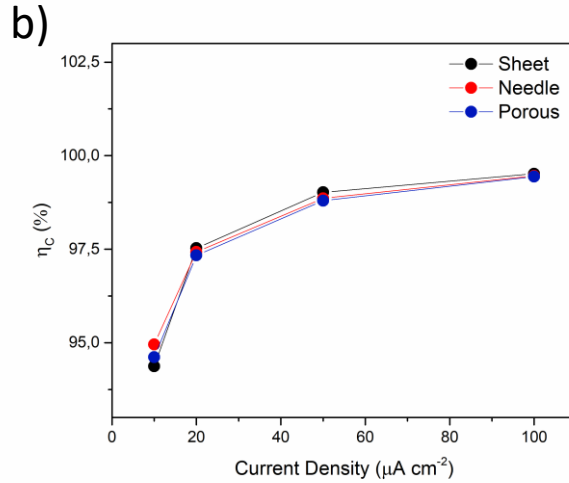
b)

Figure 2. Rate capability comparison between different morphologies evaluated in a GCD test at different current densities: 10, 20, 50 and 100 $\mu A\ cm^{-2}$, at a maximum cell voltage of 3V. (a) Areal capacitance *vs* current density and (b) coulombic efficiency at those rates.

The results are shown **Figure 2**, where areal capacitance and coulombic efficiency *vs* the current density are displayed in Figures 2a and 2b, respectively. From this test the performance difference in terms of areal capacitance between the different morphologies is even more evident. From the capacitance retention point of view, the trend is identical with Needle, Sheet and Porous devices displaying a reduction of approximatively 60%, 65% and 70%, respectively. Concerning the coulombic efficiency, it was always greater than 90% with no evident distinction. In **Figure 3**, we show the energetic properties of the devices based on LIG electrodes obtained with different laser parameters. This Ragone plot was built from the GCD test carried out at different current rates and 3V maximum cell voltage. All the three types of devices fall in the region >1$\mu Wh\ cm^{-2}$ at low power levels, as obtained also by Lin et al. with BMIM BF4.[8] The different power capability might be addressed to different electrolyte conductivities and also LIG electrical properties of the written geometry. Cyclability tests were also performed in galvanostatic mode at 20 $\mu A\ cm^{-2}$ current density and the results are shown in Figure S5 together with the coulombic efficiency. It was observed that the initial capacitance of LIG electrode is about 2.55 mF cm^{-2}, and gradually decrease to

11

1.62 mF cm^{-2} during the first 500 cycles, but nearly no obvious capacitance decrease was observable during the next few thousands of cycles. Impressively, even after 3200 continuous charge/discharge cycles, the LIG device retains about 63% of the initial capacitance with coulombic efficiency ever higher than 97%. The initial loss might be due to parasitic reactions. Indeed, the systems retains 67% after the very first 500 cycles losing only the 4% in the last 3000. From these initial measurements, we chose the needle morphology for the next temperature dependent characterizations.

During temperature characterization, the electrochemical stability window was determined by lowering the maximum applied voltage by a value much greater than the thermal voltage corresponding to a temperature step, Δv_{th}. The reason for such a choice was related to the fact that the best performing device was chosen according to its maximum capacitance at 3V and at room temperature, neglecting the coulombic efficiency difference at the same voltage. Voltage was reduced at each temperature step by an amount of 100mV in order to evaluate the potential window at highest reachable temperature of 100°C (limit imposed by the package, in this case), then, a complete characterization was performed at a voltage rated at temperature limit throughout the temperature range.
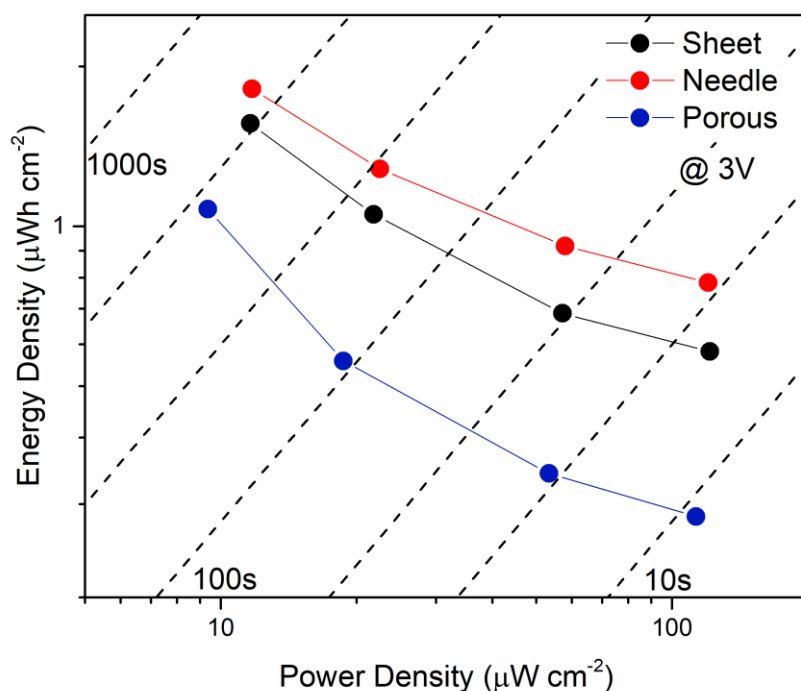
Figure 3. Ragone plot obtained for different electrode morphology derived from the GCD comparison test. Four current rates of:10, 20, 50 and 100 μA cm^{-2} at a potential window of 3V.

The results of this characterization are shown in **Figure 4**a, where we report the evolution of the 50th CV cycles recorded at different temperatures, and in Figure 4b the obtained areal capacitance and energy values. As it can be observed, there is a clear increasing trend in the areal capacitance that can be justified by an increased conductivity, of both electrodes and electrolyte, as proved by Figure 4c, in which EIS results at different temperature are reported. The inset of Figure 4c shows the high-medium frequency range. It is possible to see the presence of two semicircles with variable amplitude depending on the temperature. The whole resistive behaviour seems unchanged but the relative contribution of the two semicircles could be due to the temperature dependency of the interface between the LIG and aluminium current collector and the LIG/electrolyte one.[20,21] The fitting of both contributions is reported in Table S1. These results allowed us to confirm the overall qualitative behaviour of the

13

device. Finally, an improvement of the charge transport along the LIG network was expected.[22]
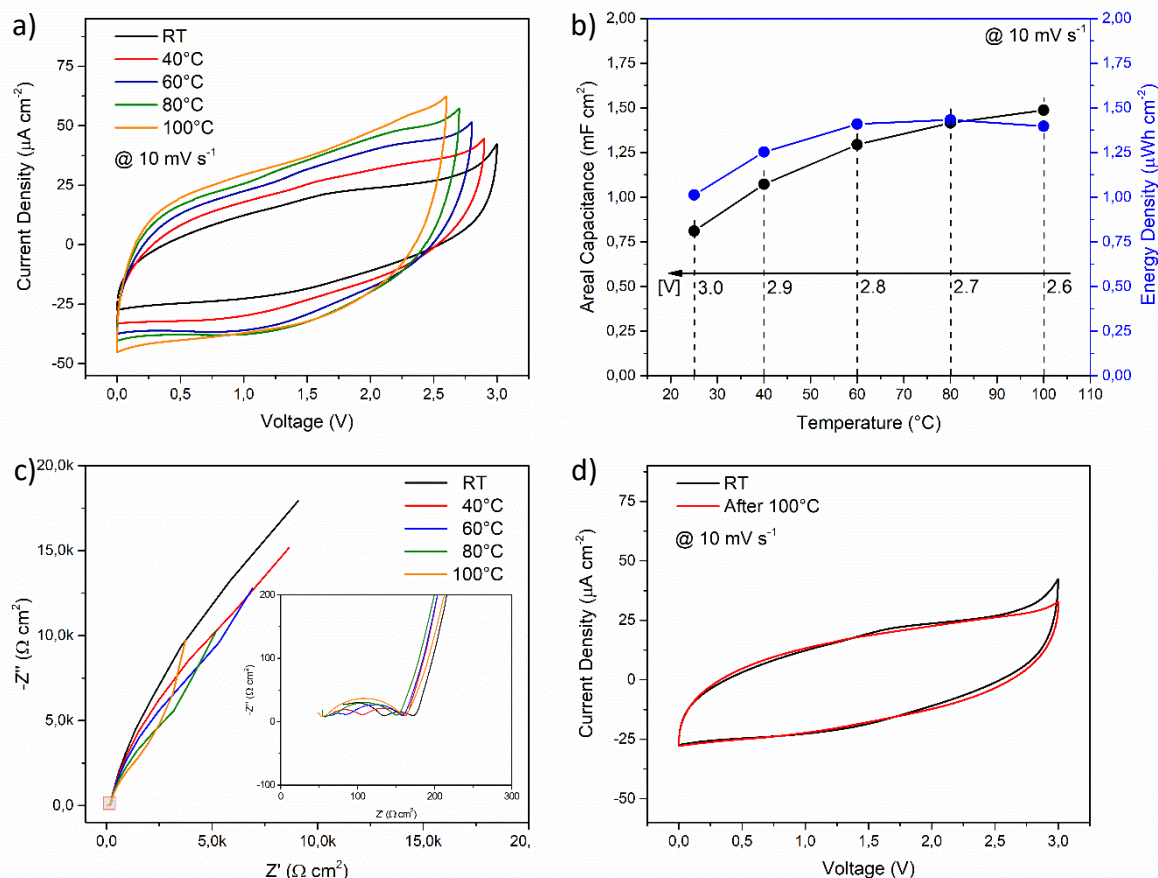

Figure 4. Electrochemical characterization of the needle-morphology devices at different temperatures: RT, 40, 60, 80 and 100 °C. CV was employed to study the voltage stability of the device at as shown in (a), at 10 mV s^{-1}. In (b) the derived quantities from CV measurements while in (c) a comparison between Nyquist plots obtained at the different temperatures. In (d) a comparison between CV results before and after the tests at 100°C.

It is evident, however, that the capacitance increase does not balance the voltage window reduction leading to a non-monotone trend for the energy with temperature. However, the overall energy variation after the maximum recorded at 80°C is negligible with respect to the increase from room temperature value (less than 3% versus an increase of almost 43%).

Finally, as shown in Figure 4d, the unchanged voltammetric response before and after the high temperature test evidence that the onset of the electrolyte degradation was avoided. From the CV analysis in temperature we determined that the maximum voltage window that can be exploited in the full temperature range is 2.6 V. Thus, this value was used to perform the following GCD characterization at different temperatures (see **Figure 5**). In Figure 5a we report the evolution rate capability as function of temperatures (GCDs performed at 10, 20, 50 and 100 $\mu A\ cm^{-2}$). It has to be said that 10 $\mu A\ cm^{-2}$ is a very low value since it required several minutes for the device to be completely charged and discharged. However, such a low rate can be exploited to retrieve practical information concerning applicative purposes (such as a lower limiting current value). Indeed, as reported in Figure 5b, the system efficiency decreases at lower rates and higher temperatures meaning that losses phenomena are promoted at high temperatures (due to leakage currents).

This is further proved by the leakage current measurements carried out at RT and 100 °C, which show the increase of the current with temperature, as reported in Figure S6. As a matter of fact, a very low value of leakage current is measured at RT (<0.15 $\mu A\ cm^{-2}$) with respect to the one rated at 100°C (of approximatively 3.83 $\mu A\ cm^{-2}$). Nevertheless, this inefficiency does not affect the discharge capacitance, which increased with temperature and remained quite stable through the 50 cycles per current rate.
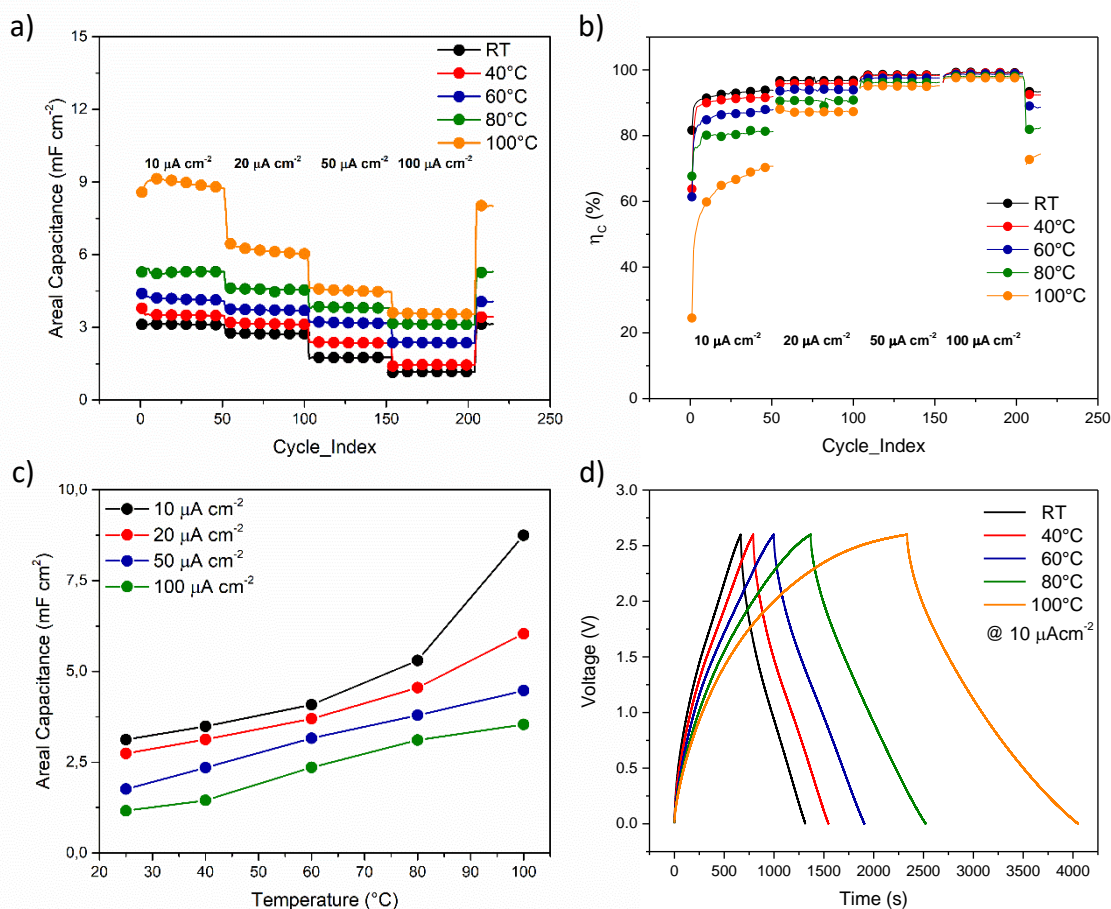
Figure 5. Electrochemical characterization of the needle morphology devices at different temperatures: RT, 40, 60, 80 and 100 °C at de-rated voltage of 2.6 V. GCD was employed to study the device rate capability at different temperatures as shown in (a). (b) coulombic efficiency vs. cycle number, (c) areal capacitance versus temperature trend at different rates and (d) a comparison between GCDs results at 10 µA cm^{-2} at different temperatures.

This result is confirmed in Figure 5c and better appreciated in Figure 5d. If the analysis had been conducted at higher voltage values within the same temperature window, it could have turned into a less stable device with pronounced capacitance fading. Finally, the authors would like to highlight that the system cycled at least 2 days at the lowest current rate at 100°C without experience any damage.
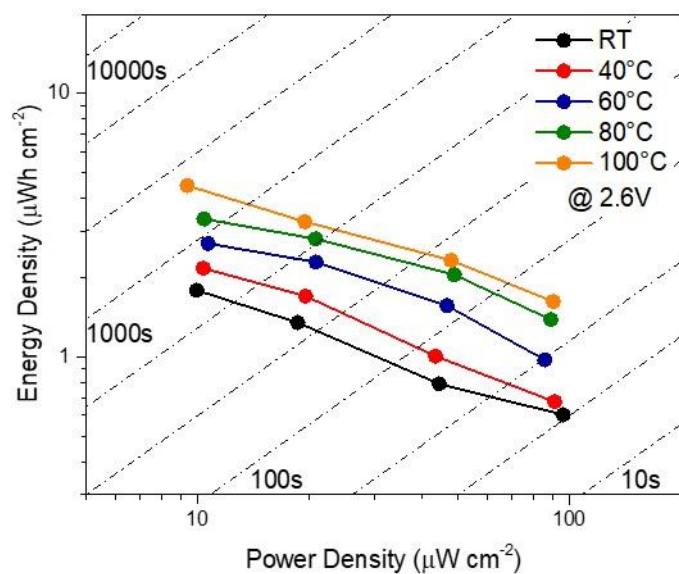
Figure 6: Ragone plot obtained for different temperatures derived from the GCD test carried out at 2.6V, four current rates of:10, 20, 50 and 100 µA cm^{-2}.

The Ragone plot was built from GCD experiments performed at de-rated voltage and shown in **Figure 6**. As it can be observed, the overall energy density increases with temperature without affecting the power capability of the device. These results are in accordance with literature as well as promising. In the work of Lin and co-workers they rated 1µWh cm^{-2} with BMIM BF4 with a voltage window of 3V at a power level of 1mW cm^{-2}. Such a high-power value can be addressed to the different ILs having higher conductivity and different electrode resistance due to the different electrode architecture. However, there here proposed device was able to triplicate the energy density by increasing the temperature from RT up to 100°C. Finally, bending test were performed in view of flexible application as in the case of wearable electronics or harsh environments in which often the encumbrance must be reduced and the device customized to curvy surfaces. For this purpose, devices were assembled in a slightly different way with respect to the steps proposed in Figure S2. Indeed, glass slides were removed, and devices were assembled directly on the pouch cell sheet. Electrochemical

17

characterizations described ahead were repeated up to a bending radius of 1.25 cm. The results show no substantial differences at low scan rates (see **Figure 7**a), and even an improved capacitance retention at higher scan rates.
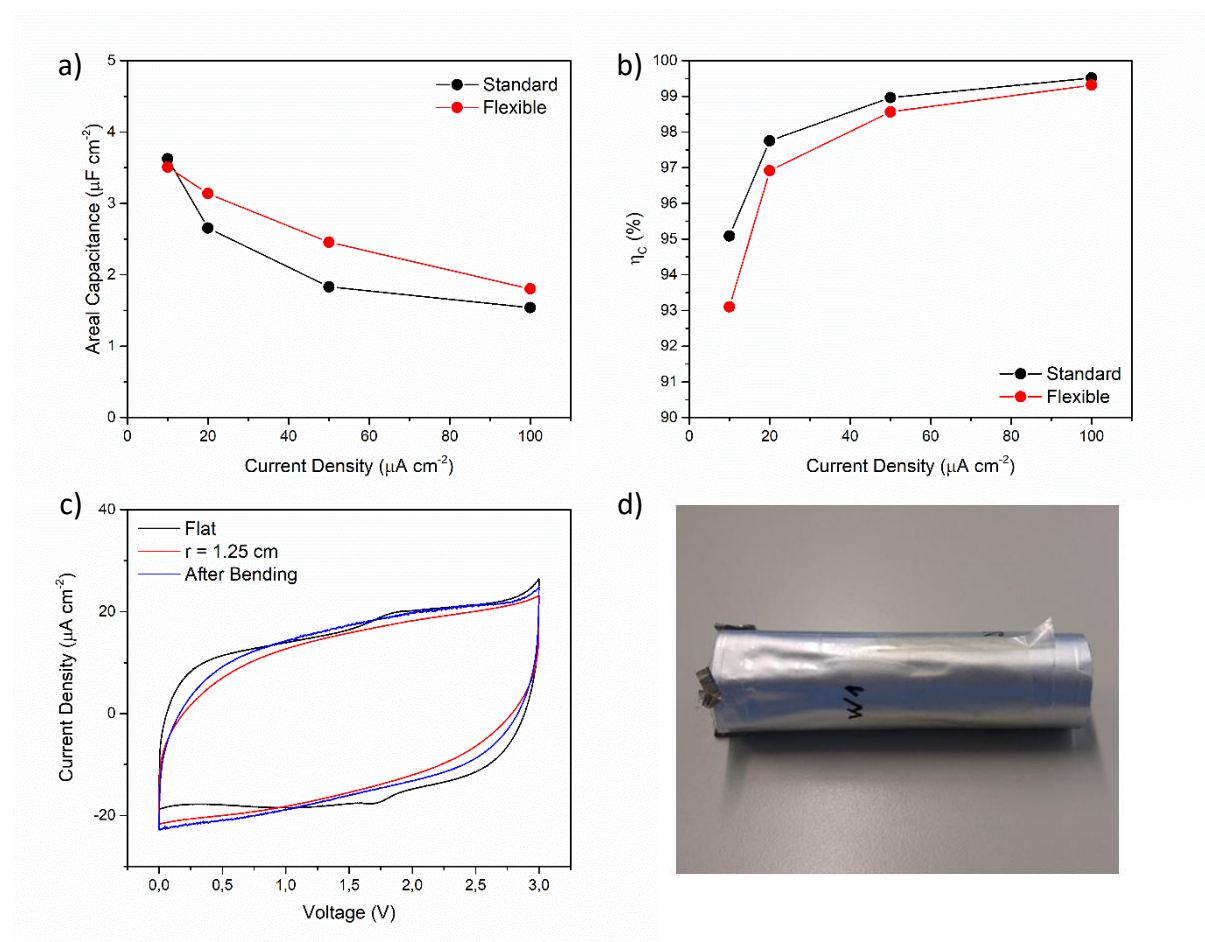

Figure 7: Bending test results and comparison with planar devices. In a) Areal capacitance versus current densities and b) respective coulombic efficiencies. In c) CV profiles carried out at 10 mV s^{-1} in which it is possible to appreciate a minor capacitance loss upon bending. d) A picture of the bent device.

Although the coulombic efficiency seems to be slightly affected by the bending (Figure 7b), the shape of the cyclic voltammogram after the bending test appears highly comparable, demonstrating the flexibility does not compromise its function.

4. Conclusions

18

In conclusion, an innovative and rational combination of materials such as laser-induced graphene and ionic liquid was reported for the fabrication of high temperature and flexible supercapacitor.

The physico-chemical properties of the LIG were modified by acting on the laser parameters, strongly affecting the electrochemical performance of the electrode and resulting in a maximum areal capacitance of 3.7 mF cm^{-2} as measured by GCD at 10 µA cm^{-2}. The device retained up to 75% of the capacitance after 3200 cycles with a coulombic efficiency always higher than 97% and an extremely low value of leakage current (<0.15 µA cm^{-2}). By increasing the temperature up to 100°C the performance of the device was improved, with only a small variation of the voltage window, achieving energy and power density as high as 4.8 µWh cm^{-2} and 90 µW cm^{-2}, respectively.

Finally, the response of the flexible architecture of the device exhibit promising results retaining almost 90% of its initial capacitance after rolling up with a low curvature radius. Moreover, the de-rated voltage analysis demonstrates that by reducing the maximum cell voltage for a wide operative temperature range avoid compromise supercapacitors energetic performances.

References

1. Kyeremateng, N. A.*, et al.*, *Nature Nanotechnology* (2017) **12** (1), 7
2. Beidaghi, M., and Gogotsi, Y., *Energy and Environmental Science* (2014) **7** (3), 867
3. Johnson, R. W.*, et al.*, *IEEE Transactions on Electronics Packaging Manufacturing* (2004) **27** (3), 164
4. Watson, J., and Castro, G., *Journal of Materials Science: Materials in Electronics* (2015) **26** (12), 9226
5. Lin, R.*, et al.*, *J. Phys. Chem. Lett.* (2011) **2** (19), 2396
6. Lewandowski, A.*, et al.*, *Journal of Power Sources* (2010) **195** (17), 5814

7.   Balducci, A*., et al.*, *Journal of Power Sources* (2007) **165** (2), 922

8.   Lin, J*., et al.*, *Nature Communications* (2014) **5**

9.   Lamberti, A*., et al.*, *Nanotechnology* (2017) **28** (17)

10.   Guoping Xiong, A. K., Timothy S. Fisher, *Thermal Effects in Supercapacitors*. Springer: Cham, 2015

11.   Zhang, L*., et al.*, *Renewable and Sustainable Energy Reviews* (2018) **81**, 1868

12.   Hibino, T*., et al.*, *Scientific Reports* (2015) **5**

13.   Hastak, R. S*., et al.*, *Electrochimica Acta* (2012) **59**, 296

14.   Bockris, J. O. M., Electrodics. In *Modern Electrochemistry 2A*, Springer, Boston, MA, (2002)

15.   Liu, H*., et al.*, *Journal of Power Sources* (2015) **285**, 303

16.   Li, J*., et al.*, *Electrochimica Acta* (2016) **197**, 84

17.   Huang, H. C*., et al.*, *Journal of Materials Chemistry A* (2014) **2** (36), 14963

18.   Shen, C*., et al.*, *Journal of Microelectromechanical Systems* (2017) **26** (5), 949

19.   Parmeggiani, M*., et al.*, *ACS Applied Materials and Interfaces* (2019) **11** (36), 33221

20.   Portet, C*., et al.*, *Electrochimica Acta* (2004) **49** (6), 905

21.   Pan, H. L*., et al.*, *Chinese Physics B* (2011) **20** (11)

22.   Fang, X. Y*., et al.*, *Physics Letters, Section A: General, Atomic and Solid State Physics* (2015) **379** (37), 2245